Journal of Power Sources 249 (2014) 110–117

Contents lists available at ScienceDirect

Journal of Power Sources

journal homepage: www.elsevier.com/locate/jpowsour

In situ monitoring of discharge/charge processes in Li–O_2 batteries by electrochemical impedance spectroscopy

Imanol Landa-Medrano [a], Idoia Ruiz de Larramendi [a], Nagore Ortiz-Vitoriano [a,b,1], Ricardo Pinedo [a], José Ignacio Ruiz de Larramendi [a], Teófilo Rojo [a,b,*]

[a] Departamento de Química Inorgánica, Universidad del País Vasco UPV/EHU, Apdo. 644, 48080 Bilbao, Spain
[b] CIC energiGUNE, Parque Tecnológico de Álava, Albert Einstein 48 Edificio CIC, 01510 Miñano, Spain

HIGHLIGHTS

- Two Li–O_2 cells have been investigated through impedance spectroscopy.
- An electrochemical model for Li–O_2 batteries is proposed.
- Model allows in situ investigation of the fundamental electrochemical mechanisms.

GRAPHICAL ABSTRACT

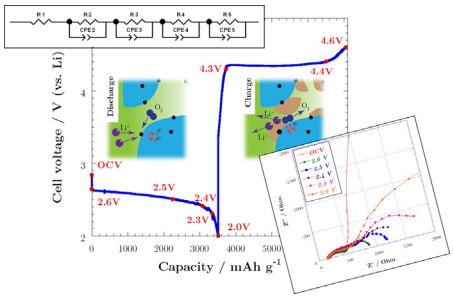

ARTICLE INFO

Article history:
Received 8 August 2013
Received in revised form
14 October 2013
Accepted 17 October 2013
Available online 25 October 2013

Keywords:
Li–O_2batteries
Battery performance
Electrochemical impedance spectroscopy
Discharge products

ABSTRACT

Gaining insight into the reaction mechanisms underway during charge and discharge in Li–air batteries is essential to allow the target development of improved power and performance devices. This work reports the in situ monitoring of Li–air cells by electrochemical impedance spectroscopy and, for the first time, the development of an electrochemical model allowing the identification and attribution of the processes involved. The voltage at which each reaction product forms has been identified, including Li_2O_2 or Li_2CO_3 during discharge, together with the delithiation of the outer part of Li_2O_2 and oxidation reactions and electrolyte decomposition. The developed model can be used as a valuable tool for the optimisation of composition and structure of the air electrode through the investigation of the resistance associated with each process.

1. Introduction

Energy storage has attracted a great deal of interest from the scientific community since the beginning of 19th century when the first battery prototypes were developed. These electrochemical devices have long been considered the most promising alternative for energy storage due to advantages including, but not limited to, direct energy conversion without intermediate steps, high efficiency, no moving parts, very little contamination, easy transportation. From the late 20th century, however, all these advantages became part of our daily life with the commercialisation of lithium ion batteries and their application in mobile devices such as phones and laptops. Despite the many advantages of this technology, new energy demands have emerged that require energy density higher than that possible with lithium ion batteries. One of the major challenges is the application of electrochemical energy storage in the automotive field. It is precisely in this area

* Corresponding author. Departamento de Química Inorgánica, Universidad del País Vasco UPV/EHU, Apdo. 644, 48080 Bilbao, Spain. Tel.: +34 94 6012458; fax: +34 94 6013500.
E-mail addresses: teo.rojo@ehu.es, trojo@cicenergigune.com (T. Rojo).
[1] Present address: Electrochemical Energy Laboratory, Massachusetts Institute of Technology, Cambridge, MA 02139, USA.

0378-7753/$ – see front matter © 2013 Elsevier B.V. All rights reserved.
http://dx.doi.org/10.1016/j.jpowsour.2013.10.077

where metal–air batteries seem capable of playing an important role in the development of electric vehicles [1,2]. In fact Li–air batteries can produce gravimetric energy densities between 3 and 5 times higher than Li-ion batteries [3–5]. In its common configuration, the Li–air battery comprises a lithium-containing anode (currently Li-metal), a lithium-conducting organic electrolyte and an air cathode. Cell discharge occurs when the Li metal anode electrochemically oxidises and the Li^+ ions migrate across the electrolyte to the cathode. At the cathode, oxygen reduction occurs (*oxygen reduction reaction*, ORR) and lithium peroxide (Li_2O_2) is then formed as the final discharge product in a reaction between the Li^+ and O_2^{2-}. The reaction will take place until exhaustion of lithium, oxygen or until lithium oxides occupy all the active sites where the reaction occurs. The reactions taking place during battery discharge are:

$$Li \rightarrow Li^+ + e^- \text{ (anode reaction)}$$

$$2Li^+ + O_2 + 2e^- \rightarrow Li_2O_2 \text{ (cathode reaction)}$$

$$2Li + O_2 \rightarrow Li_2O_2 \text{ (global reaction)}$$

In addition to lithium peroxide, lithium oxide is usually formed. Its presence is undesirable due to the difficulty of decomposition during charging. It is formed by the following reaction:

$$2Li + \tfrac{1}{2}O_2 \rightarrow Li_2O$$

During charge the above reactions will reverse, playing a key role the lithium oxide dissociation (lithium peroxide mainly) and the oxidation of peroxide anions (*oxygen evolution reaction*, OER).

There are several limitations, however, that prevent the use of these devices, such as slow kinetics of the ORR occurring during discharge and OER during charge [6]. It has therefore been found that the use of catalysts can influence the performance of these batteries [7,8]. A thorough understanding of the fundamental mechanisms of the cathode reactions is therefore vital to enhance the efficiency and capacity of rechargeable Li–air batteries.

In order to study these processes, in addition to common electrochemical characterisation techniques, X-ray photoelectron spectroscopy (XPS), Raman spectroscopy and transmission electron microscopy (TEM) have proved to be fundamental techniques for in situ monitoring of reaction products that take place during charge and discharge [9–11]. The problems associated with these techniques stem from the requirement for high vacuum and a solid electrolyte, neither of which are the case in reality.

Another technique which has been widely used in electrochemical devices is electrochemical impedance spectroscopy (EIS), by which it is possible to analyse the mechanisms and kinetics of the processes involved, in situ [12]. To date this technique has rarely been used as a monitoring tool for electrochemical processes in metal–air batteries. In other types of devices such as fuel cells [13] or Li–S batteries [14], however, it has proven to be very useful for the study of reaction products and interfaces. It would therefore be very useful for the study of Li–air batteries. The quantification of these products and the thorough understanding of the reactions taking place, both at surface and bulk, are considered one of the key points for the development of new materials to enable the implementation of these energy storage systems.

Some authors have reported impedance spectra but only pre- and post-cycling or during discharge/charge processes but without proposing an electrochemical model to explain the obtained results and allow the direct analysis of the charge/discharge process evolution [15–18]. These analyses show the increase of the observed semicircles after cell discharge. This increase is associated with the formation of the most insulating discharge product Li_2O_2 [15–19]. H. Kitaura et al. also analysed the charge process and determined, by means of EIS, the degradation of the cell after charging it at high potentials (5 V) [17]. In addition, these studies have also shown the increase of the resistance when solid electrolytes are employed [18] or when the LiOH concentration decreases [16]. In order to solve these limitations, the increase of the operation temperature to 60 °C has been proposed [16,18].

In this work, a more exhaustive analysis of the charge–discharge processes has been performed by electrochemical impedance spectroscopy leading to the proposal of an electrochemical model for Li–air batteries. The spectra obtained for a range of cells at several voltages in the discharge and charge processes have been analysed. The influence of the different processes is discussed with focus on the limiting steps.

2. Experimental

The oxygen electrode consisted of carbon black (C-Nergy™ Super C-65, 64 $m^2\ g^{-1}$) and polytetrafluoroethylene (PTFE) binder (Sigma–Aldrich) in a weight ratio of 90:10. Ethanol was used as a dispersing agent to form a slurry that was stirred overnight. The slurry was air-brushed over a stainless steel mesh (Alfa Aesar®), which works as cathode current collector, and left to dry for a week in air. Finally, 10 mm diameter electrodes were punched, leading to carbon masses between 0.3 and 0.6 mg per electrode.

Swagelok-type cells were used to perform the electrochemical measurements. The battery consisted of a Li metal foil over stainless steel, acting as anode and current collector respectively, a glass fibre separator (Whatman), 12 drops of $LiClO_4$ 0.1 M in dimethoxyethane (DME – Sigma–Aldrich, 99.5%) as the electrolyte and the previously described oxygen cathode. The cell assembly was carried out inside a glove box with Ar flux. For the electrochemical measurements, the argon was replaced by oxygen inside the cell. A constant flux of oxygen was introduced at the cathode side for 30 min in order to purge the Ar, and after this time the cell, containing a sufficient oxygen amount, was closed. Fig. 1 shows a schematic representation of the cell used for the electrochemical measurements.

The Li–O_2 cells were cycled between 2 and 4.6 V at room temperature at a current density of 0.15 mA cm^{-2}, using a Biologic-sas VMP control potentiostat. The impedance spectra were recorded in the frequency range between 10^6 and 0.01 Hz with perturbation amplitude of 10 mV. Impedance spectra were analysed using Scribner Associates' Zview software.

Charge and discharge product characterisation was carried out by X-ray powder diffraction (XRD), using a Phillips PW1710 diffractometer using Cu Kα radiation. The analysis was performed with a scanning step of 0.02° over the angular range 25–55° and

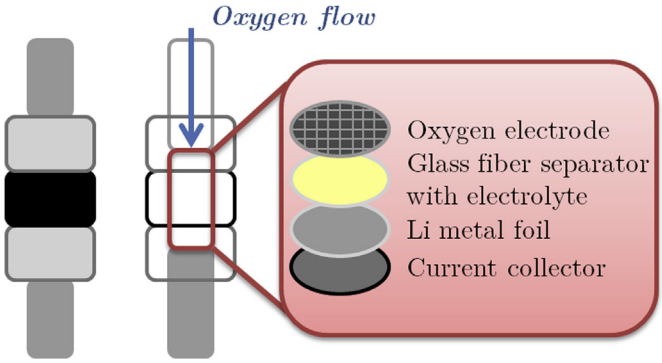

Fig. 1. Schematic representation of the Swagelok-type cell used for the measurements.

the obtained data were fitted using the FULLPROF program [20]. The morphology of the electrodes and the reaction products were examined by scanning electron microscopy (SEM) using a Hitachi S-4800 microscope at 20.0 kV accelerating voltage. X-ray photoelectron spectroscopy (XPS) was performed in an SPECS (Berlin, Germany) system equipped with a Phoibos 150 1D-DLD analyzer and monochromatic Al Kα radiation (1486.6 eV). An initial analysis of the present elements was carried out at wide scan mode (step energy 1 eV, dwell time 0.1 s, pass energy 40 eV) and after that, high-resolution spectra of the found elements were acquired (step energy 0.1 eV, dwell time 0.1 s, pass energy 20 eV) with an electron take-off angle of 90°. The binding energy of the adventitious carbon (C1s) was set at 284.6 eV to correct sample charging. The spectra were fitted with the CasaXPS 2.3.16 software, which models the Gauss-Lorentzian contributions, after background subtraction (Shirley).

3. Results and discussion

Several nominally identical cells have been studied in order to develop an electrochemical model to monitor in situ the electrochemical processes taking place in the cell. In this work the results obtained for the 2 cells employed in the development of the electrochemical model are presented. This model has been applied to similar systems obtaining similar results which ensures the reproducibility of the method.

The cells were stopped after the first discharge (D cell) and one cycle (D–C cell) to characterise the reactions taking place and products formed. Fig. 2 shows the capacity curves obtained for both cells in pure oxygen. After the first discharge the capacity values of D and D–C cells were 2662 and 3511 mAh g^{-1}, respectively. These capacity values are in good agreement with those reported by other authors [21–24]. A discharge plateau is observed at 2.6 V and its slope increases up to the cutoff of 2 V. The plateau obtained during charge is more stable and occurs between 4.3 and 4.4 V. The overvoltage of cell 2 is 1.9 V.

The air electrodes were evaluated using X-ray diffraction (XRD) before testing and after the discharge process for D cell and discharge/charge process for D–C cell. XRD patterns are shown in Fig. 3. Teflon (binder) and stainless steel (mesh) peaks can be observed for the pristine electrode by XRD. In addition to the materials mentioned above, peaks corresponding to $LiClO_4$ (electrolyte precipitate), SiO_2 (remnants of the separator adhered to the electrode) and discharge products such as Li_2O_2 and Li_2CO_3 can be found for the other diffractograms. It is worth noting that these discharge products were not completely eliminated during charge, with traces found by XRD, a consequence of electrolyte evaporation. The amount of Li_2O_2 and Li_2CO_3 in the electrode after the charge is, however, much lower in proportion to those obtained after device discharge.

The discharge products were also characterised by complementary techniques. Scanning electron microscopy (SEM) was used to study the morphology and location of the products. Fig. 4 shows the images where the discharge products are observed at the oxygen electrode. These images were taken of the carbon accumulated inside the pores of the mesh and clearly show the presence of secondary discharge phases, similar to those obtained by McCloskey et al. [25]. The morphology of these discharge products is also consistent with those reported by Adams et al., who relate this morphology to measurements performed at current densities above 25 μA cm^{-2} [26].

The attained discharge products have also been analysed by means of X-ray photoelectron spectroscopy. The analyses were performed on the cathode side exposed to the oxygen where the discharge products are mainly located due to the low solubility of

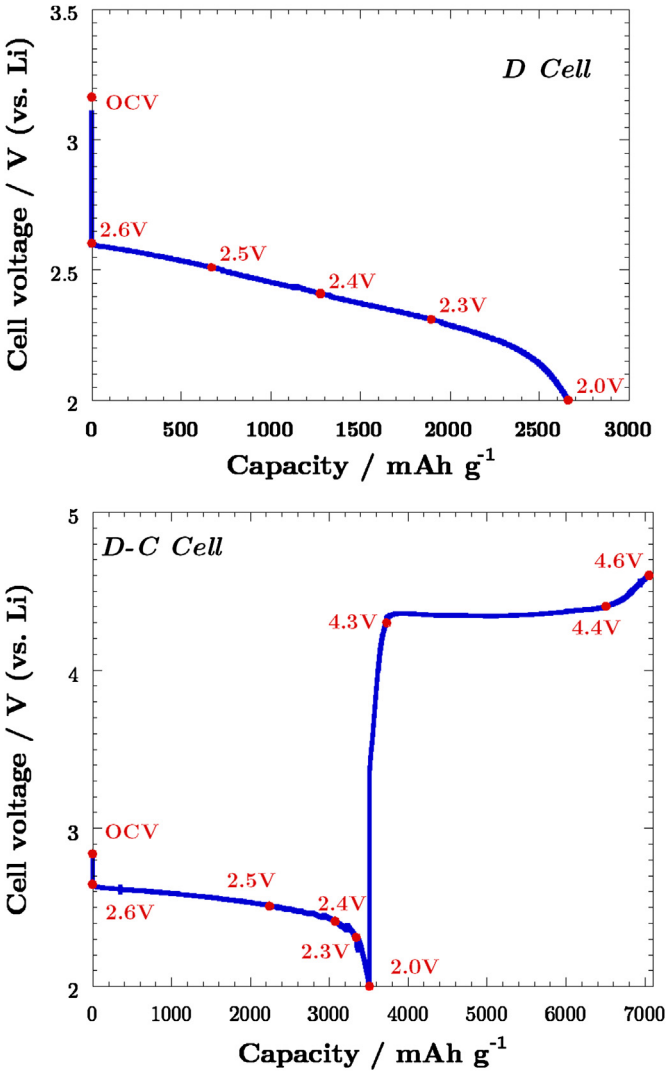

Fig. 2. Discharge and discharge/charge curves of D and D–C cells. Voltages where impedance measurements were carried out are indicated.

oxygen in DME (8.76 mol m^{-3}) [27]. The obtained Li 1s, O 1s and C 1s spectra are shown in Fig. 5. From these spectra it can be deduced that the main discharge product at this electrode side is Li_2O_2. Nevertheless, a certain amount of Li_2O_2 has evolved to Li_2CO_3 during the discharge process. In addition, $LiClO_4$ can also be found as a consequence of the solvent evaporation. These results are in good agreement with the discharge products observed by means of X-ray diffraction.

In order to monitor the processes taking place in the battery, the following voltages were selected for EIS measurement: OCV, 2.6, 2.5, 2.4, 2.3, 2.0 V during discharge, and 4.3, 4.4 and 4.6 V during charge, as shown in Fig. 2. The impedance spectra for both cells are presented in Fig. 6. At high frequencies (~10^3 Hz) only one semicircle is observed for both cells at OCV due to the high resistance associated with the processes at low frequencies (~1 Hz), with only the processes ascribed to diffusion observable. For the remaining voltages, however, a second semicircle appears at low frequencies. High and low frequency semicircles each consist of several contributions as their centres are shifted below the real axis, making analysis more difficult. The accurate differentiation of these contributions, however, is considered a key factor for the development of an equivalent circuit model capable of simulating and explaining the electrochemical processes taking place in the

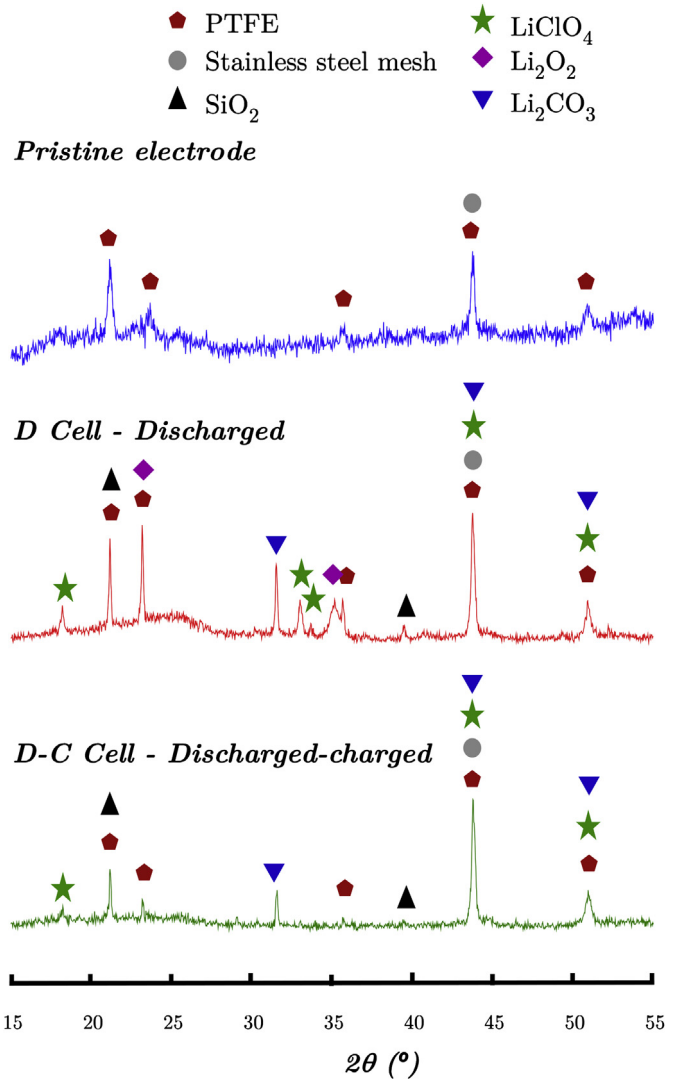

Fig. 3. X-ray diffractograms obtained for the following electrodes: without testing, after discharge (D cell) and after one discharge/charge cycle (D–C cell).

cell. The first step towards the achievement of this goal focuses on discerning the number of processes taking place at each voltage. This can be better analysed through the use of Bode plots (Fig. 7). The Bode plot of cell 1 shows the presence of two processes at high (10^3 Hz) and low frequencies (10 Hz). Asymmetric peaks are observed for both cells suggesting the presence of multiple processes at high and low frequencies. It is possible to distinguish two processes at high frequencies and another two at low frequencies. The processes at high and low frequencies occur at constant frequency values for both cells during discharge (10^3 and 10 Hz respectively), whereas during charging, for the D–C cell, the high frequency process shifts to lower frequencies (10–100 Hz). This can be associated with the formation and/or precipitation of secondary reaction products at the electrolyte/electrode interface, increasing their resistances. This fact is explained in more detail later. The analysis of the low frequency region of the impedance spectra during charge is more complicated due to the strongly overlapping processes and limitation of the data measured. The developed model for the discharge processes, however, will be applied to the charge processes in order to provide validation. The overlapping of Bode and Nyquist plots at OCV and 2.6 V for both cells at high frequencies (10^2–10^6 Hz) reveals that no reaction has occurred in the cell. In turn, at voltages lower than 2.6 V, where the discharge plateau starts, the resistance associated with high frequencies (R_{HF}) increases up to a maximum when the discharge finishes (2.0 V). Regarding the charging processes in cell 2, R_{HF} remains constant between 2.0 and 4.3 V (where no reaction is observed) and increases to 4.4 V, and then remains constant for the end of the charge. The resistance associated with low frequency processes (R_{LF}) increases during discharge between 2.6 and 2.3 V, up to a maximum at 2.0 V, and during charge a decrease of R_{LF} is observed. The presence of discharge products at the cathode surface reduces the active cathode area, limiting the ORR, as will be seen later.

As discussed previously, through the analysis of the Bode plots it is possible to distinguish two processes at high and two at low frequencies, however these two processes are overlapping. Fig. 8 shows a schematic of the proposed electrochemical model (R_1–R_2CPE$_2$–R_3CPE$_3$–R_4CPE$_4$–R_5CPE$_5$). The first element, R_1, is associated with the ohmic resistance, which includes the electrolyte contribution (physical and chemical changes), current collectors and cell contacts and its numerical value is calculated from the high frequency intercept on the Z′ axis. The four subsequent elements in series consist of a resistor (R) in parallel with a constant phase element (CPE) (R||CPE). Each of these R||CPE elements must be associated with a process in order to validate the proposed model.

The constant phase element (CPE) is a simple distributed element which produces impedance having a constant phase angle in the complex plane [28,29]. A CPE is often used in a model in place of a capacitor to compensate the non-homogeneity in a system. For example, a rough or porous surface can cause a double-layer capacitance to appear as a constant phase element with a CPE-P value between 0.9 and 1. In fact, a capacitor is actually a constant phase element – one with a constant phase angle of 90°. From the impedance associated with each CPE element, $Z = 1/T(j\omega)^P$ (where ω is the angular frequency and T and P are constants), it is possible to obtain the degree of distortion of the impedance spectrum. When $P = 1$ the CPE will act as a capacitor and T will be its capacity

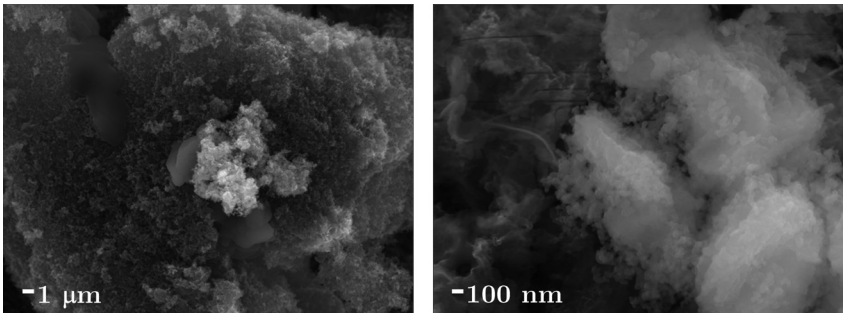

Fig. 4. SEM images of discharge secondary phases formed at the oxygen exposed side at different magnifications.

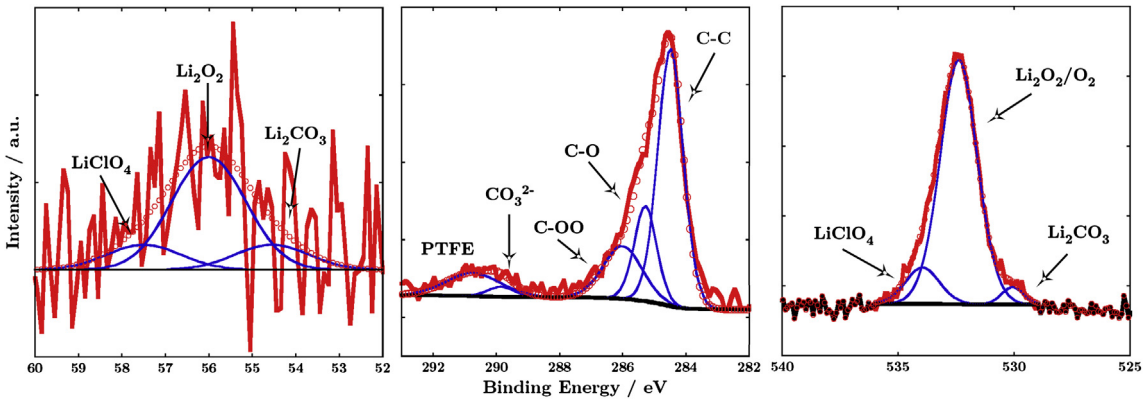

Fig. 5. Li 1s (left), O1s (middle) and C 1s (right) XPS data collected on the cathode surface exposed to oxygen.

value. In this study, the P value is between 0.556 and 1. For the fitting of OCV, 4 and 5 data processes were replaced by a finite length Warburg element, used when charge carriers diffuse through a material. Lower frequencies correspond to diffusion deeper into the material. If the material is thin, low frequencies will penetrate the entire thickness, creating a finite length Warburg element. Fig. 9 presents some of the fittings obtained with the equivalent circuit shown in Fig. 8. These fittings are representative of the rest of the data obtained. The model fits well with the experimental data from the studied cells, for both discharge and charge. In function of the charge or discharge depth, the low frequency processes are overlapped which makes the fitting difficult. When analysing these results, the individual resistances (R_4 and R_5) as well as the sum of both ($R_4 + R_5$) will be taken into account. The obtained results for the resistances of the equivalent circuit at different voltages for both cells are presented in Fig. 10. The ohmic resistance remains constant, only showing a small drop for the D–C cell. The changes associated with the ohmic resistance are normally due to the chemical and physical properties of the electrolyte. It is widely known that the solvent used to dissolve $LiClO_4$ (DME) tends to evaporate with time [30]; this gives rise to a decrease in the electrolyte thickness which results in small changes in R_1. The high frequency processes have been fitted through the deconvolution of two processes. R_2 presents low resistance values remaining constant during the study of the cell. The capacitance value of CPE_2 is 10^{-7} F, which can be associated with charge transference at the anode surface (anode/electrolyte interface). Changes in R_2 are not appreciable but this is expected to increase during cycling due to the formation of dendrites at the anode surface or the formation of Solid Electrolyte Interphase (SEI) layer [31,32]. The capacitance value of CPE_3, observed at high frequencies, is on the order of 10^{-6} F. This contribution is ascribed to charge transference through the electrolyte/cathode interface [23]. Kichambare et al. also ascribed the resistances associated to the high frequency semicircle to charge-transfer processes and a higher resistance was obtained when discharge products were deposited on the pores of the cathode [33]. R_3 remains constant up to the discharge plateau (2.60 V) when it sharply increases. This behaviour is due to the formation of reaction products when the discharge plateau is reached, as has been reported by other authors [18,27,34]. The reactions taking place during discharge include the formation of the following products:

$$Li^+ + O_2 + e^- \rightarrow LiO_2 \quad (I)$$

$$2LiO_2 \rightarrow Li_2O_2 + O_2 \quad (II)$$

$$4Li^+ + O_2 + 4e^- \rightarrow 2Li_2O \quad (III)$$

$$Li_2O_2 + 2e^- + 2Li^+ \rightarrow 2Li_2O \quad (IV)$$

It is believed that the reaction mechanism at discharge involves the intermediate formation of lithium superoxide [Eq. (I)] which is short lived (about 5–10 min) in the presence of Li cations and further reacts to form lithium peroxide [Eq. (II)] [18]. It is likely that other reaction routes resulting in the formation of lithium oxide are also present [Eqs. (III) and (IV)]. No remaining lithium oxide was found by XRD throughout this study. Several authors have reported the formation of Li_2CO_3 at the air electrode during discharge in systems with ether-based electrolytes [10,23,35,36]. These carbonates are formed during discharge at the carbon/electrolyte interface due to the chemical reactivity of Li_2O_2 and electrolyte decomposition [36,37]. The formation of reaction products with low conductivity values [$\sigma(Li_2O_2) = 2\cdot10^{-13}$ S cm^{-1}; $\sigma(Li_2CO_3) = 5\cdot10^{-9}$ S cm^{-1}] block the electrolyte/cathode interface increasing the resistance associated with those processes (R_3). In addition, it is known that throughout charge and discharge cycles, the solvent used in the electrolyte evaporates; this causes a shift at the interface cathode/electrolyte/gas interface and the precipitation of lithium salt ($LiClO_4$) which has been identified by XRD. The presence of this at the cathode/electrolyte interface increases the resistance at high voltages during charge. In addition, at high voltages electrolyte decomposition occurs, which can contribute to the increase of R_3 at potentials higher than 4.4 V.

R_4 and R_5 contributions are ascribed to oxygen diffusion from outer atmosphere to air-electrode surface and oxygen dissociative adsorption together with the charge-transfer resistance of electrochemical reduction of oxygen species. The contributions at lower frequencies are normally associated with lithium and oxygen diffusion controlled processes [15,33]. CPE_4 and CPE_5 capacitance values are on the order of 10^{-4} F, which is in good agreement with the described electrochemical processes. The reduction reaction is as follows:

$$O_2 + e^- \rightarrow O_2^- \quad (V)$$

During discharge, a gradual increase of the contribution associated with these electrochemical processes (oxygen reduction) is observed for both cells, becoming the dominant process in the electrochemical response. During charge, however, these resistances decrease, implying that the oxidation process is favoured as the voltage increases. As the charge progresses, the products formed during discharge are decomposed by the following reactions:

$$Li_2O_2 \rightarrow 2Li^+ + O_2 + 2e^- \quad (VI)$$

$$Li_2CO_3 \rightarrow 4Li^+ + 2CO_2 + 4e^- \quad (VII)$$

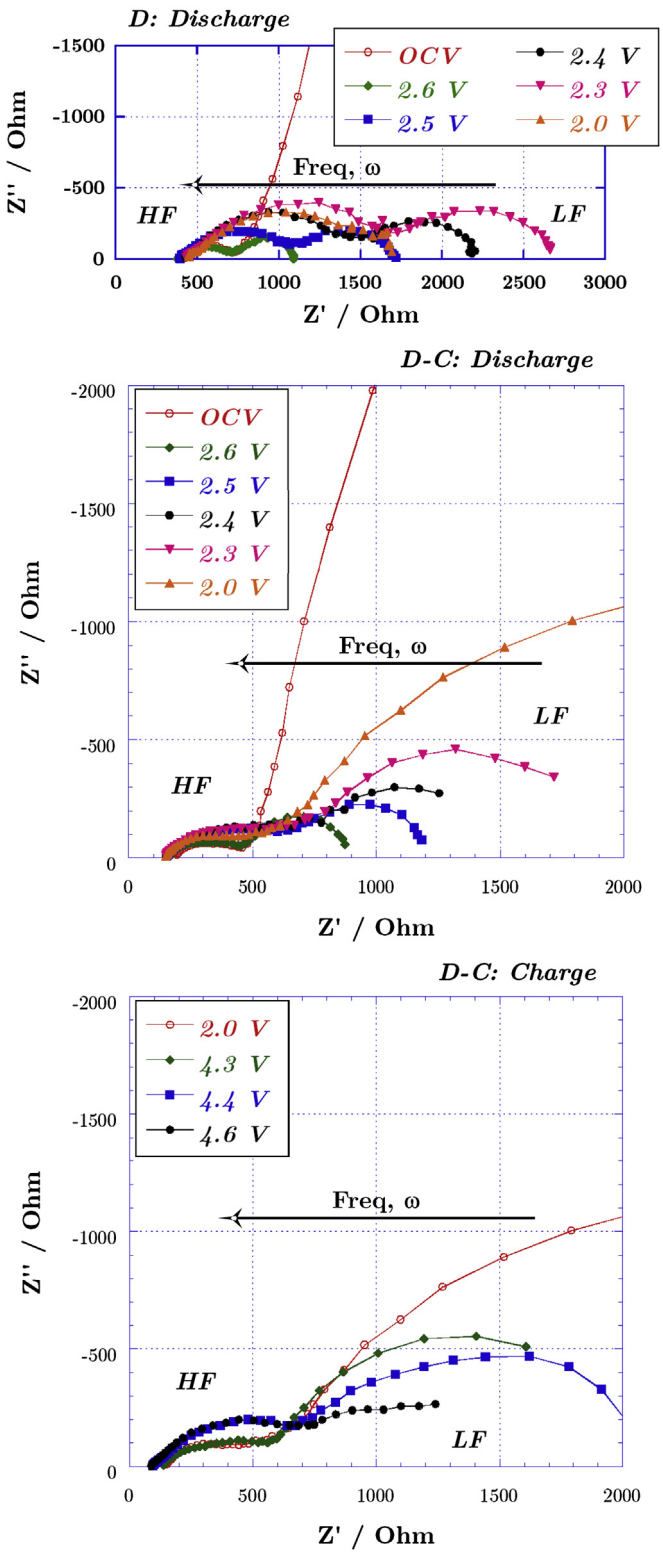

Fig. 6. Nyquist plots of impedance response of D and D–C cells at indicated voltages (HF: high frequencies; LF: low frequencies).

After the charging process, the resistance ($R_4 + R_5$) associated with the air electrode does not return to its initial value. This is possibly related to residual traces of Li_2O_2 and Li_2CO_3 discharge products on the air electrode which have not fully decomposed. The presence of these agglomerates at the cathode surface will lead to greater resistance values due to the reduction of active

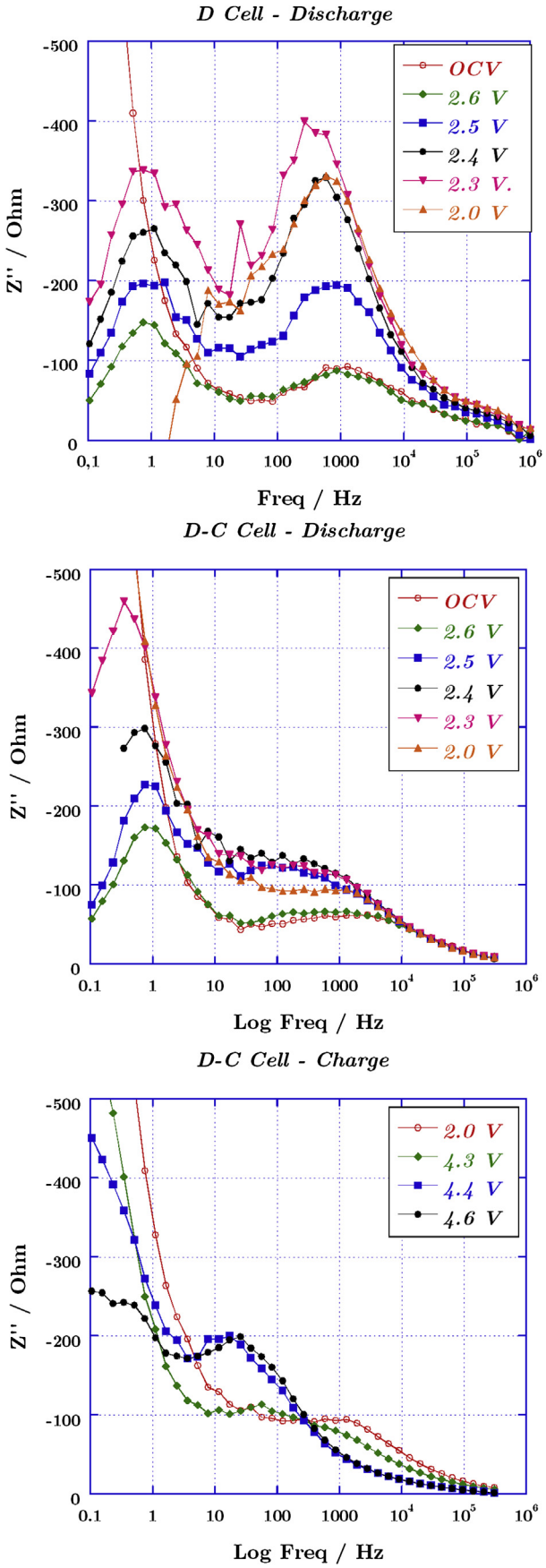

Fig. 7. Bode plots of impedance response of D and D–C cells at selected voltages.

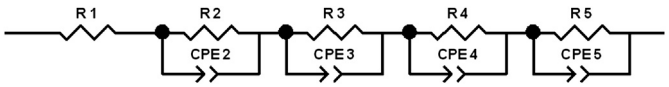

Fig. 8. Schematic of the proposed equivalent circuit.

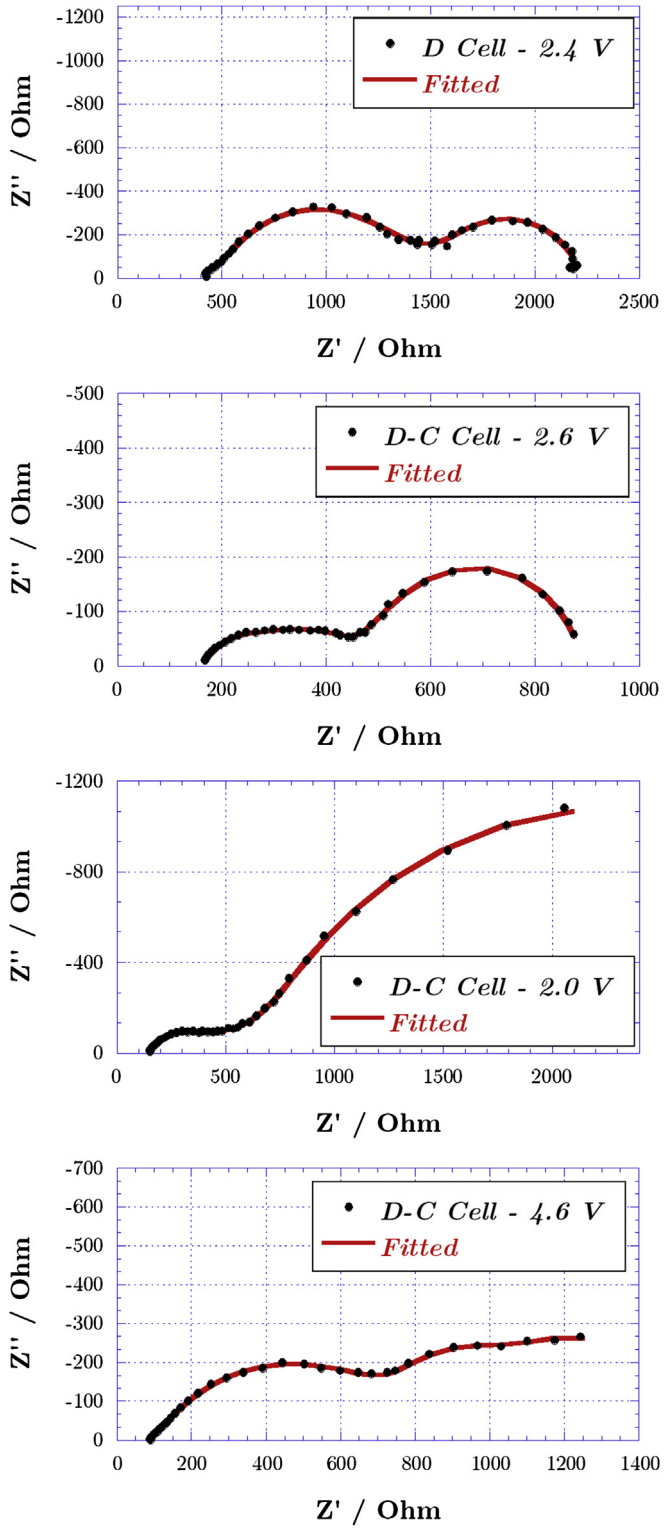

Fig. 9. Fitting of the impedance spectra using the proposed equivalent circuit.

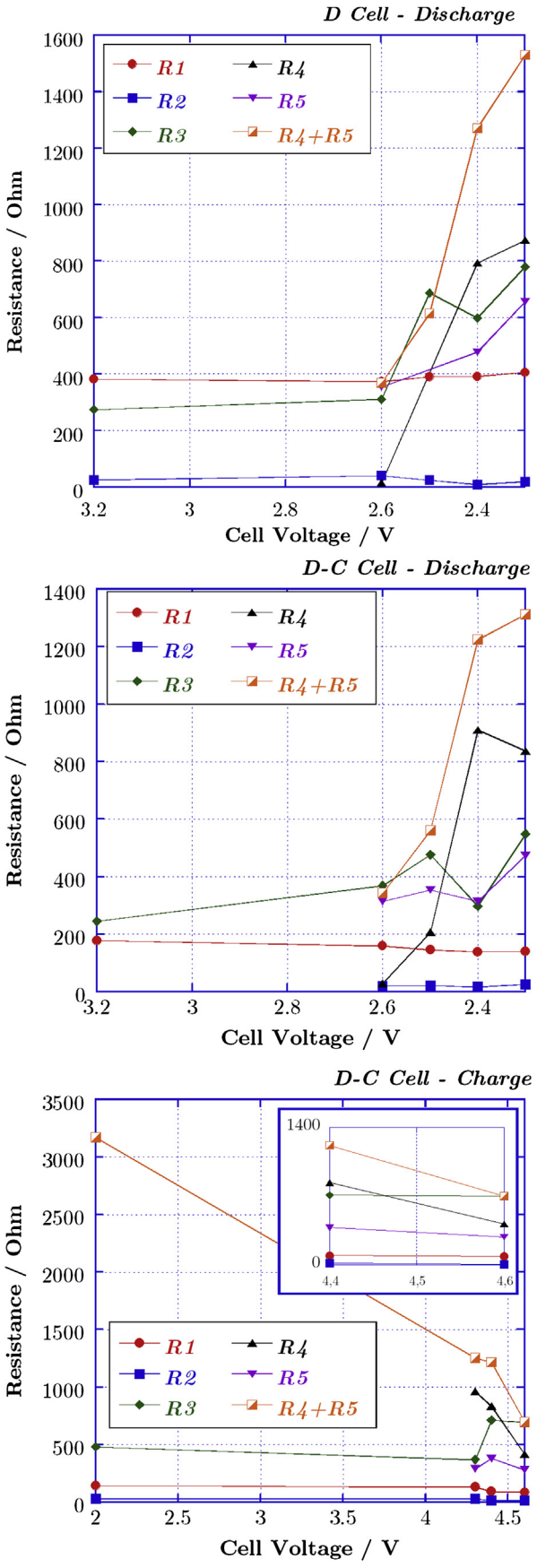

Fig. 10. Resistances obtained using the fitting of the impedance data to the equivalent circuit proposed in this work.

cathode area, limiting the ORR. In addition, the low conductivity of Li_2O_2 will limit the kinetic reduction of ORR [11]. Recently, Lu et al. have reported the possible reaction occurring during charge [6]. This study shows that in the first phase of the charging process, lithium deintercalation occurs, leading to diffusion-dominated processes. Considering the evolution of the resistances at low frequencies, the observed decrease between 2 and 4.3 V for R_5 is in good agreement with the activation of diffusion in the system. At the charge plateau (4.3–4.4 V) Li_2O_2 oxidation will take place, decreasing R_4. Finally, between 4.4 and 4.5 V decomposition of Li_2CO_3 will take place, releasing Li^+ and CO_2, as confirmed by McCloskey et al. [35]. The decomposition of these insulating carbonates leads to a decrease in R_4 resistance. At the same time, a small decrease in R_5 resistance occurs due to the increase of diffusion of charge carriers. Based on these results, it is possible to assign the processes associated with R_4 to Li_2O_2 bulk oxidation and with R_5 to diffusion processes. Further studies are needed, however, in order to identify the precise reaction mechanisms and intermediate products of these processes.

It is likely that the use of catalysts in the electrode such as Pt, Ru or MnO_2 will lead to a decrease in R_4 resistance at intermediate frequencies during charging. It is well known that the use of these materials can decrease the activation barrier of the processes associated with OER. The resistances associated with reduction or oxidation processes, which are dominant in this study and contribute to a lower performance of Li–air batteries, will decrease with the use of catalysts.

4. Conclusions

Two cells have been investigated by electrochemical impedance spectroscopy, one during discharge and another during both discharge and charge at a range of voltages. An impedance model based on an equivalent circuit has been proposed, for the first time, which has been validated for discharge and charge processes. This equivalent circuit model consists of the following elements in series: R_1–R_2CPE$_2$–R_3CPE$_3$–R_4CPE$_4$–R_5CPE$_5$. R_1 is associated with the ohmic resistance, which includes the electrolyte contribution, current collectors and cell contacts. The subsequent elements in series consist of a resistor in parallel with a constant phase element. R_2CPE$_2$ and R_3CPE$_3$ are ascribed to anode/electrolyte and electrolyte/cathode interface processes, respectively. The latter contribution increases in resistance on discharge, as the reaction products form, and decreases on charging due to their decomposition. At high voltages a small increase in the resistance associated with formation of salt of the electrolyte is observed. Finally, the last two processes are related to electrochemical reactions associated with the ORR and OER. Applying this model to Li–air batteries will allow the in situ investigation of the fundamental electrochemical mechanisms of the different components, as well as allow the evaluation of the behaviour of cathode catalysts through the analysis of their effect on the resistance associated with ORR and OER.

Acknowledgements

This work has been partially financed by the Ministerio de Educación y Ciencia under project MAT2010-19442 and the Eusko Jaurlaritza/Gobierno Vasco under projects IT-570-13, SAIOTEK (S-PE11UN064 and S-PE12UN140) and ETORTEK (ENERGIGUNE'12 – IE12-335). I. Landa-Medrano thanks the Universidad del País Vasco (UPV/EHU) for his predoctoral fellowship. N. Ortiz-Vitoriano thanks the Universidad del País Vasco (UPV/EHU) for funding her research activities under the "Especialización de Personal Investigador del Vicerrectorado de Investigación de la UPV/EHU" programme. The authors thank the technicians of SGIker for the XPS measurements.

References

[1] M. Armand, J.-M. Tarascon, Nature 451 (2008) 652.
[2] G. Girishkumar, B. McCloskey, A.C. Luntz, S. Swanson, W. Wilcke, J. Phys. Chem. Lett. 1 (2010) 2193.
[3] P.G. Bruce, S.A. Freunberger, L.J. Hardwick, J.M. Tarascon, Nat. Mater. 11 (2012) 19.
[4] R. Black, B. Adams, L.F. Nazar, Adv. Energy Mater. 2 (2012) 801.
[5] H.-G. Jung, J. Hassoun, J.-B. Park, Y.-K. Sun, B. Scrosati, Nat. Chem. 4 (2012) 579.
[6] Y.-C. Lu, Y. Shao-Horn, J. Phys. Chem. Lett. 4 (2013) 93.
[7] Y.-C. Lu, Z. Xu, H.A. Gasteiger, S. Chen, K. Hamad-Schifferli, Y. Shao-Horn, J. Am. Chem. Soc. 132 (2010) 12170.
[8] Y.-C. Lu, H.A. Gasteiger, Y. Shao-Horn, J. Am. Chem. Soc. 133 (2011) 19048.
[9] R. Younesi, M. Hahlin, F. Björefors, P. Johansson, K. Edström, Chem. Mater. 25 (2013) 77.
[10] Y.-C. Lu, B.M. Gallant, D.G. Kwabi, J.R. Harding, R.R. Mitchell, M.S. Whittingham, Y. Shao-Horn, Energy Environ. Sci. 6 (2013) 750.
[11] L. Zhong, R.R. Mitchell, Y. Liu, B.M. Gallant, C.V. Thompson, J. Yu Huang, S.X. Mao, Y. Shao-Horn, NanoLett. 13 (2013) 2209.
[12] N. Ortiz-Vitoriano, A. Hauch, I. Ruiz de Larramendi, C. Bernuy-López, R. Knibbe, T. Rojo, J. Power Sources 239 (2013) 196.
[13] N. Ortiz-Vitoriano, C. Bernuy-López, I. Ruiz de Larramendi, R. Knibbe, K. Thydén, A. Hauch, P. Holtappels, T. Rojo, Appl. Energy 104 (2013) 984.
[14] Z. Deng, Z. Zhang, Y. Lai, J. Liu, J. Li, Y. Liu, J. Electrochem. Soc. 160 (2013) A553.
[15] M. Eswaran, N. Munichandraiah, L.G. Scanlon, Electrochem. Solid-State Lett. 13 (2010) A121.
[16] P. He, Y. Wang, H. Zhou, J. Power Sources 196 (2011) 5611.
[17] H. Kitaura, H. Zhou, Energy Environ. Sci. 5 (2012) 9077.
[18] T. Zhang, H. Zhou, Nat. Commun. 4 (2013) 1817.
[19] C. Xia, C.L. Bender, B. Bergner, K. Peppler, J. Janek, Electrochem. Commun. 26 (2013) 93.
[20] J. Rodriguez-Carvajal, Physica B 192 (1993) 55.
[21] J. Christensen, P. Albertus, R.S. Sanchez-Carrera, T. Lohmann, B. Kozinsky, R. Liedtke, J. Ahmed, A. Kojic, J. Electrochem. Soc. 159 (2012) R1.
[22] S. Monaco, F. Soavi, M. Mastragostino, J. Phys. Chem. Lett. 4 (2013) 1379.
[23] S.A. Freunberger, Y. Chen, N.E. Drewett, L.J. Hardwick, F. Bardé, P.G. Bruce, Angew. Chem. Int. Ed. 50 (2011) 8609.
[24] C.K. Chan, H.L. Peng, G. Liu, K. McIlwrath, X.F. Zhang, R.A. Huggins, Y. Cui, Nat. Nanotechnol. 3 (2008) 31.
[25] B.D. McCloskey, D.S. Bethune, R.M. Shelby, G. Girishkumar, A.C. Luntz, J. Phys. Chem. Lett. 2 (2011) 1161.
[26] B.D. Adams, C. Radtke, R. Black, M.L. Trudeaus, K. Zaghib, L.F. Nazar, Energy Environ. Sci. 6 (2013) 1772.
[27] U. Sahapatsombut, H. Cheng, K. Scott, J. Power Sources 227 (2013) 243.
[28] J.R. Macdonald, Solid State Ionics 13 (1984) 147.
[29] R.L. Hurt, J.R. Macdonald, Solid State Ionics 20 (1986) 111.
[30] Y. Cui, Z. Wen, X. Liang, Y. Lu, J. Jin, M. Wu, X. Wu, Energy Environ. Sci. 5 (2012) 7893.
[31] R. Younesi, M. Hahlin, M. Roberts, K. Edstroem, J. Power Sources 225 (2013) 40.
[32] R.S. Assary, J. Lu, P. Du, X. Luo, X. Zhang, Y. Ren, L.A. Curtiss, K. Amine, ChemSusChem. 6 (2013) 51.
[33] P. Kichambare, J. Kumar, S. Rodrigues, B. Kumar, J. Power Sources 196 (2011) 3310.
[34] J. Hassoun, F. Croce, M. Armand, B. Scrosati, Angew. Chem. Int. Ed. 50 (2011) 2999.
[35] B.D. McCloskey, A. Speidel, R. Scheffler, D.C. Miller, V. Viswanathan, J.S. Hummelshøj, J.K. Nørskov, A.C. Luntz, J. Phys. Chem. Lett. 3 (2012) 997.
[36] B.M. Gallant, R.R. Mitchell, D.G. Kwabi, J. Zhou, L. Zuin, C.V. Thompson, Y. Shao-Horn, J. Phys. Chem. C 116 (2012) 20800.
[37] F. Li, T. Zhang, H. Zhou, Energy Environ. Sci. 6 (2013) 1125.